Indian Journal of Pure & Applied Physics
Vol. 62, July 2024, pp. 576-592
DOI: 10.56042/ijpap.v62i7.7859

Spectroscopic, Computational, Docking and Cytotoxicity Studies on 2-(2-Chlorophenyl)benzimidazole as a Potent Anti-breast Cancer Agent

V S Kunjumol[a], S Jeyavijayan[b*], N Karthik[b] & S Sumathi[b]

[a]Department of Engineering, University of Technology and Applied Science, Shinas 324, Oman

[b]Department of Physics, Kalasalingam Academy of Research and Education, Krishnankoil, Tamil Nadu 626 126, India

Received 7 January 2024; accepted 1 May 2024

The 2-(2-Chlorophenyl)benzimidazole (CPBZ) vibrational assignments were performed using FT-IR and FT-Raman spectroscopy. The ideal geometrical parameters, IR intensity, and Raman activity of the vibrational bands of CPBZ were determined using the B3LYP functional and 6-311++G(d,p) level of theory, and the findings are compared with experimental findings. To comprehend the charge distribution within the molecule, the Mulliken charges, HOMO-LUMO energies, and molecular electrostatic potential (MEP) are computed. The molecular orbital contributions were evaluated using the total density of states (TDOS). To assess the electronic charge on each atom and the bond order between a pair of atoms, studies on the natural bond orbital (NBO) and the Fukui function were all examined. The 1H and 13C NMR chemical shifts were calculated using gauge-independent atomic orbital (GIAO). The structure and bioactivity of the molecule were validated by the docking research of CPBZ with the breast cancer inhibitors 1A28, 1ERE, 1AQU, and 1M17. The molecule's drug applicability has been determined by using ADMET prediction. Additional research has been done on the molecule's cytotoxicity and antibacterial properties. Ultimately, it appears that CPBZ has promise as a pharmacological option for treating breast cancer.

Keywords: DFT; 2-(2-Chlorophenyl) benzimidazole; Cytotoxicity; Docking; Breast cancer

1 Introduction

Heterocyclic compounds known as benzimidazoles are produced by the combination of imidazole with benzene. Because they have two nitrogens as heteroatoms, they are more powerful, useful compounds for medicine, and extensive biochemicals. Numerous non-covalent interactions, including hydrogen bonding, coordination, ion-dipole, cation-stacking, hydrophobic effect, and van der Waals force, can enable the special benzene-fused imidazole ring to swiftly link with a range of active targets in biological systems[1,2]. Significant biological and pharmacological effects of benzimidazole derivatives have been shown in the medical field; these effects include antibacterial[3], antifungal[4], anti-inflammatory[5], antiviral[6], antihelmintic[7], and anticancer[8]. In particular, benzimidazole and its derivatives have been increasingly popular in recent years as cancer therapies[9–13]. Because they have varying oxidation states and interact with many hazardous compounds, they make it possible to produce medications in the field of pharmacology with significant therapeutic potential. 5-nitrobenzimidazole has been the subject of recent studies employing the DFT Approach to examine structural, spectroscopic, NBO, and molecular docking[14]. Density functional theory (DFT) has emerged as a powerful technique for interpreting vibrational spectra of moderately large molecules in recent years. DFT has attracted a lot of attention because it applies to chemical systems more quickly than traditional quantum mechanical correlation methods[15]. A careful examination of the literature indicates that a complete theoretical or experimental investigation of 2-(2-Chlorophenyl)benzimidazole (CPBZ) has not yet been conducted.

Therefore, in order to discover significant chemical characteristics, spectroscopic studies using FTIR, FT-Raman, and UV-Vis have been conducted for CPBZ and DFT/6-311++G(d,p) simulations in the current work. Experimentally obtained spectroscopic data was confirmed by DFT calculations. To find out more about CPBZ's charge transfer inside molecules, the lowest unoccupied (LUMO) and highest occupied (HOMO) molecule orbital energies have been computed. The purpose of measuring CPBZ's molecular electrostatic potential (MEP) was to find out more about the nucleophilic and electrophilic sites. The total density of states (TDOS), partial density of states (PDOS), and overlap population (OPDOS) spectra have all been used to study the

*Corresponding author: (E-mail: sjeyavijayan@gmail.com)

overlapping of molecular orbitals. In order to comprehend the interactions between the complex and the atoms that surround it in the molecule, natural bond orbitals (NBO) were also presented. In order to determine the molecule's bioactivity, several methods such as the Fukui function, Mulliken population analysis, and global reactivity relations[16] were investigated. Atomic orbital theory has been used to compute the theoretical 13C and 1H NMR. Many biological characteristics have been attained, such as antibacterial activity, cytotoxicity, and ADMET (Absorption, Distribution, Metabolism, Excretion, and Toxicity) characteristics. Additionally, docking experiments have been conducted to ascertain the biological activity of the CPBZ molecule against breast cancer (for protein-ligand interaction). By considering the aforementioned factors, the current effort aims to provide full molecular vibrations, geometry, and biological properties of CPBZ.

2 Experimental and Computation

2.1 Experimental Characterizations

For spectral measurements, 2-(2-Chlorophenyl) benzimidazole (CPBZ), which was acquired from Sigma-Aldrich Company as a fine sample, was used. A Perkin-Elmer RX1 spectrophotometer fitted with an MCT detector, KBr beam splitter, and globar source was used to record the Fourier transform infrared spectrum (FTIR) of CPBZ in the 50-4000 cm^{-1} range. Next, using a computer interfaced BRUKER RFS 27 model interferometer with a resolution of 2 cm^{-1} at the 1064 nm line of a Nd:YAG laser by 200 mW output power excitation, the sample was exposed to record the FT-Raman spectrum in the 50-4000 cm^{-1} region. The sample's UV absorption spectrum was measured between 100 and 500 nm using a UV-Vis spectrophotometer (UV-2600) and ethanol as a solvent.

2.2 Quantum Computational Details

Density functional theory was utilized in conjunction with the 6-311++G(d,p) level basis set to optimize the ground state molecular structure of the CPBZ utilizing the Becke-3-parameter-Lee-Yang-Parr (B3LYP) functional[17,18]. The computations were performed using GAUSSIAN 09 software[19]. By scaling the B3LYP approach with a scaling factor of 0.9613, the scaled quantum mechanical (SQM) methodology guarantees a satisfactory comparability between the experimental and DFT vibrational frequencies[20]. The results of the GAUSSVIEW program were combined with symmetry considerations to provide vibrational frequency allocations with a high degree of accuracy. The MOLVIB Program (Adaptation V7.0-G77) from Sundius is used to determine the potential energy distribution (PED%) for different frequency modes[21]. The contributions of molecular orbitals in the different functional groups of the molecule were calculated using the GaussSum 3.0 tool[22].

2.3 Molecular Docking and ADMET

Molecular docking is a highly valuable tool for studying protein-ligand interactions. The relationship between CPBZ and proteins that indicate breast cancer was the main focus of this study. In the present docking analysis, the CPBZ molecule was utilized as the ligand, and the targeted breast cancer proteins were the human progesterone receptor (PDB ID: 1A28), human estrogen receptor (PDB ID: 1ERE), estrogen sulfotransferase receptor (PDB ID: 1AQU), and epidermal growth factor receptor (PDB ID: 1M17). The target proteins' three-dimensional (3D) coordinates were obtained by using the Protein Data Bank (http://www.pdb.org)[23]. Before molecular docking, we used Discovery Studio[24] (2017 R2 client version) to examine the structures of proteins and amino acids. One of the public ligand databases[25], PubChem (http://pubch em.ncbi.nlm.nih.gov), was used to derive the structure of the ligand CPBZ. The process of docking CPBZ with breast cancer indicators was then carried out via the MGL Tools-1.5.4 package interface with Autodock Vina[26] (Adaptation: 4.2.1). To ascertain the pharmacodynamic activities of CPBZ in the human body, we employed an online software program called the ADMET (absorption, distribution, metabolism, elimination, and toxicity) prediction tool[27] (http://lmmd.ecust.edu.cn/admetsar2/) in this work.

2.4 MTT Based Cytotoxicity Assay

The MCF-7 breast cancer cell lines were donated by the National Centre for Cell Sciences (NCCS), which is situated in Pune, India. 10% FBS (fetal bovine serum) and DMEM (Dulbecco's Modified Eagle Media) were used to sustain the cell line. To ensure there was no bacterial contamination, 100 U/ml of penicillin and 100 µg/ml of tetracycline were given to the medium. The cell lines' 37 °C medium was continuously maintained humid with 5% CO_2.

The yellow 3-4,5-dimethylthiozol-2-Yl)-2,5-diphenyltetrazoliumbromide (MTT) is reduced by the mitochondrial dehydrogenase of living cells, producing an apparent purple formation product. Living cells include NADPH-dependent reductase, which converts the MTT reagent into formazan, a dark purple material. The formazan crystals are then dissolved in the solubilizing solution, and the absorbance at 500–600 nm is measured using a plate reader. 50 mg of MTT dye and 10 ml of phosphate buffered saline (PBS) were employed in the solution. After a minute of vortexing, 0.45 microfilters were used to filter it. MTT was light-sensitive, thus light was blocked by wrapping the container with aluminium foil. The preparation was stored in a 4 °C freezer. To evaluate the anti-cancer efficaciousness of sample CPBZ, several doses were administered to MCF-7 cells.

2.5 Bacterial Strain Preparation

The antibacterial properties of CPBZ were evaluated against both Gram-positive and Gram-negative bacteria, including Methicillin-Resistant Staphylococcus aureus (MRSA) and Vancomycin-Resistant Enterococcus faecium (VREF). Gram-negative bacteria included Escherichia coli, Serratia, and Klebsiella. Nutrient Agar (NA) medium was used to pre-culture both Gram-positive and Gram-negative bacteria, which were then cultivated for the whole night at 37 °C on a rotating shaker. Different doses of CPBZ were tested for their antibacterial effectiveness using the agar well diffusion technique. One millilitre of newly cultured bacteria was pipetted into the centre of a sterile Petri plate. The mixture was then applied to the Petri plate along with Muller Hinton Agar (MHA), and allowed to set. Following the setting process, 6 mm sterile cork borer holes were drilled into agar plates that contained inoculums. After that, bacteria were put on an MHA-coated plate and let to dry. The sample CPBZ was dissolved at 0.6 mg/ml in 50% DMSO (dimethyl sulfoxide) as a reference solution, and each concentration was added to a separate well. After that, the plates were incubated at 37 °C for a further 18 hours. To test the antibacterial activity, the diameter of the wells after the inhibitory zone was incubated was examined.

3 Results and Discussion

3.1 Molecular Structure Analysis

Using the geometry optimization technique, the most stable molecule structure was determined. Using the 6-311++G(d,p) basis set and the DFT/B3LYP method, the optimized global minimum energy for CPBZ was found to be -1070.6991 Hartrees. Fig. 1 shows the ideal bond quality structure for the CPBZ. Theoretically, the bond length and bond angle of CPBZ were ascertained by comparing the experimental XRD results with those found in Table 1. The C_1 point group of the CPBZ molecule is made up of imidazole, phenyl, and chlorine groups. The bond lengths for the C20-Cl25, C19-H24, C4-C5, N3-C2, N1-C8, and N1-H14 have been calculated to be 1.7513, 1.0825, 1.3884, 1.3094, 1.3822, and 1.0075 Å, respectively. As seen in Table 1, these values are consistent with the experimental XRD values[28] of 1.744, 0.930, 1.370, 1.313, 1.383, and 1.062 Å. The ring's nitrogen and chlorine atoms are the reason for the modest asymmetry seen in the bond angles of CPBZ. These bond angles are determined to be 120.93° (122.0° by Expt.), 119.85° (119.8° by Expt.), and 122.47° (122.4° by Expt.) for C15-C20-C19, C4-C9-C8, and C7-C8-C9. Table 2 displays the thermodynamic properties of CPBZ. The CPBZ molecule has an extreme dipole moment of 4.2681 Debye, which suggests a greater interatomic interaction. It is determined that the CPBZ has a total energy of 125.834 kcal mol^{-1} and a zero-point discrete vibrational energy of 118.2612 kcal mol^{-1}. These findings are essential to understanding CPBZ's chemical interactions.

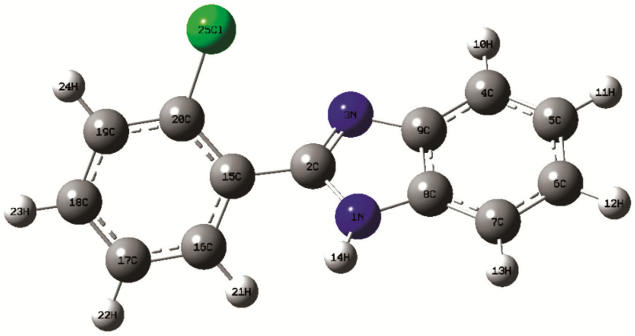

Fig. 1 — Optimized structure of 2-(2-Chlorophenyl) benzimidazole

3.2 Vibrational Assignments

There are 47 symmetric and 22 antisymmetric vibrational modes among the 69 vibrational modes of the 25 atoms in the optimized configuration. The measured FT-IR and FT-Raman frequencies for the different vibrational modes are listed in Table 3. Using the triple split valence basis set, diffuse, and polarization functions, 6-311++G(d,p), the calculated harmonic vibrational frequencies for CPBZ at the

Table 1 — Optimized structural parameters of 2-(2-Chlorophenyl)benzimidazole

Structural parameters		
Bond length (Å)	B3LYP/6-311++G(d,p)	Experimental[28]
N1-C2	1.3865	1.368
N1-C8	1.3822	1.383
N1-H14	1.0075	1.062
C2-N3	1.3094	1.313
C2-C15	1.4732	1.477
N3-C9	1.3844	1.393
C4-C5	1.3884	1.37
C4-C9	1.3994	1.401
C4-H10	1.0833	0.93
C5-C6	1.4086	1.399
C5-H11	1.0839	0.93
C6-C7	1.3905	1.365
C6-H12	1.084	0.93
C7-C8	1.3946	1.388
C7-H13	1.084	0.93
C8-C9	1.4141	1.398
C15-C16	1.4049	1.387
C15-C20	1.4048	1.393
C16-C17	1.3896	1.376
C16-H21	1.0843	0.93
C17-C18	1.3929	1.367
C17-H22	1.0835	0.93
C18-C19	1.3912	1.376
C18-H23	1.0838	0.93
C19-C20	1.3932	1.375
C19-H24	1.0825	0.93
C20-Cl25	1.7513	1.744
Bond angle (°)		
C2-N1-C8	107.15	106.7
C2-N1-H14	125.55	128.6
C8-N1-H14	126.70	124.7
N1-C2-N3	112.44	113.4
N1-C2-C15	120.58	123.2
N3-C2-C15	126.88	123.3
C2-N3-C9	105.56	104.5
C5-C4-C9	117.98	117.6
C5-C4-H10	121.76	121.20
C9-C4-H10	120.24	121.2
C4-C5-C6	121.41	121.4
C4-C5-H11	119.57	119.30
C6-C5-H11	119.00	119.30
C5-C6-C7	121.54	122.2
C5-C6-H12	119.22	118.91
C7-C6-H12	119.22	118.91
C6-C7-C8	116.71	116.5
C6-C7-H13	121.20	121.74
C8-C7-H13	122.07	121.74
N1-C8-C7	133.03	132.5
N1-C8-C9	104.48	105.1
C7-C8-C9	122.47	122.4
C4-C9-C8	119.85	119.8
C2-C15-C16	118.73	119.5
C2-C15-C20	123.63	123.2
C16-C15-C20	117.62	117.1
C15-C16-C17	121.71	121.4
C15-C16-H21	118.61	119.30
C17-C16-H21	119.63	119.31
C16-C17-C18	119.57	119.8
C16-C17-H22	119.95	119.31
C18-C17-H22	120.46	120.10
C17-C18-C19	119.93	120.8
C17-C18-H23	120.49	119.62
C19-C18-H23	119.57	119.62
C18-C19-C20	120.22	118.9
C18-C19-H24	120.67	120.54
C20-C19-H24	119.09	120.54
C15-C20-C19	120.93	122.0
C15-C20-Cl25	121.57	119.2
C19-C20-Cl25	117.46	118.8

Table 1 — Optimized structural parameters of 2-(2-Chlorophenyl)benzimidazole (*contd.*)

Table 2 — The thermodynamic parameters of 2-(2-Chlorophenyl)benzimidazole

Parameters	DFT-B3LYP/ 6-311++G(d,p)
Optimized global minimum Energy (Hartrees)	-1070.6991
Total energy(thermal), E_{total} (kcal mol^{-1})	125.834
Heat capacity, C_v (cal mol^{-1} k^{-1})	48.336
Total Entropy, S (cal mol^{-1} k^{-1})	111.003
Translational Entropy (cal mol^{-1} k^{-1})	42.175
Rotational Entropy (cal mol^{-1} k^{-1})	32.722
Vibrational Entropy (cal mol^{-1} k^{-1})	36.106
Vibrational energy, E_{vib} (kcal mol^{-1})	124.057
Zero-point vibrational energy, (kcal mol^{-1})	118.2612
Rotational constants (GHz)	
A	1.1578
B	0.2768
C	0.2352
Dipole moment (Debye)	4.2681

B3LYP level have been assembled. By contrasting the frequencies calculated at the B3LYP level with the actual values, it becomes clear that the estimated vibrational modes were overestimated due to the real system's disdain for anharmonicity. Regardless of the accuracy of the computations, it is customary to reduce the calculated harmonic frequencies by a scale factor[29] of 0.9613 in order to improve agreement with the experiment. The Figs. 2 & 3 shows the FT-IR and FT-Raman spectra of CPBZ, respectively.

Table 3 — Vibrational assignments based on PED calculations for 2-(2-Chlorophenyl)benzimidazole

S. No	Observed wave number (cm^{-1})		Wave number (cm^{-1})		IR Intensity (Km mol^{-1})	Raman activity ($Å^4$ amu^{-1})	Reduced mass (amu)	Force constant (mDyne/$Å^{-1}$)	Assignment with PED (%)
	FT-IR	FT- Raman	FT-IR	FT- Raman					
1	3520(vw)	-	3652.70	3511	51.4817	76.2342	1.0806	8.4949	νNH(99)
2	3081(vw)	-	3203.39	3079	5.1149	255.9437	1.0957	6.6247	νCH(98)
3	3071(vw)	-	3197.03	3073	12.0984	240.3950	1.0959	6.5995	νCH(97)
4	3066(vw)	3067(ms)	3193.02	3069	10.8411	161.7350	1.0947	6.5757	νCH(93)
5	3062(vw)	-	3187.37	3064	18.7095	167.0226	1.0943	6.5501	νCH(92)
6	3051(vw)	-	3179.57	3057	6.2145	87.1923	1.0899	6.4917	νCH(98)
7	3050(vw)	-	3175.85	3053	9.3661	131.3901	1.0898	6.4763	νCH(97)
8	3046(vw)	-	3170.41	3048	1.2192	34.2218	1.0863	6.4331	νCH(93)
9	3040(vw)	-	3166.16	3044	0.0288	44.4527	1.0858	6.4131	νCH(92)
10	1620(ms)	1624(vw)	1659.93	1596	8.1114	27.6570	6.7850	11.0148	νC=N(74)
11	1591(vs)	1598(vs)	1634.74	1571	3.0320	758.3548	6.2163	9.7877	νCN(74)
12	1568(ms)	1566(vw)	1619.83	1557	3.6406	11.3735	6.2432	9.6516	νCN(72)
13	1537(s)	1537(vs)	1602.97	1541	7.8394	9.0803	5.6685	8.5816	νCN(69)
14	-	1515(vw)	1571.47	1511	16.7017	918.2118	6.0857	8.8546	νCC(85)
15	1489(s)	1450(vw)	1518.26	1459	0.6198	32.9149	3.0764	4.1781	νCC(83)
16	-	1441(ms)	1502.43	1444	56.3018	4.8146	2.6219	3.4870	νCC(80)
17	-	1420(vw)	1472.82	1416	23.8627	205.9655	2.4483	3.1291	νCC(84)
18	-	1400(vw)	1457.47	1401	25.5725	91.0139	2.1201	2.6534	νCC(81)
19	1373(vs)	1350(vw)	1417.80	1363	32.1493	76.8246	2.5482	3.0180	νCC(80)
20	1315(s)	1317(vw)	1378.40	1325	46.4114	10.4981	5.4918	6.1478	νCC(85)
21	1276(vw)	1278(vs)	1333.63	1282	11.2481	26.3020	3.1145	3.2637	νCC(83)
22	-	1251(vw)	1306.83	1256	9.8135	27.4261	3.0173	3.0361	νCC(80)
23	1248(vw)	1241(vw)	1294.49	1244	35.8017	189.9092	4.0359	3.9846	νCC(84)
24	1226(vs)	-	1283.05	1233	17.7675	119.6526	1.7615	1.7085	νCC(81)
25	-	1200(vw)	1247.84	1199	3.8997	81.5197	2.5635	2.3518	νCC(80)
26	1185(ms)	-	1235.16	1187	4.0841	136.7188	1.9909	1.7896	bNH (72)
27	-	1158(w)	1187.14	1141	0.4868	13.5186	1.1045	0.9171	νCC(80)
28	1126(s)	1122(w)	1170.69	1125	0.9045	57.0967	1.1617	0.9381	bCH (76)
29	1110(vw)	-	1153.88	1109	2.5667	13.0257	1.6133	1.2656	bCH (77)
30	-	1085(vw)	1136.22	1092	2.1746	10.9211	1.5104	1.1488	bCH (75)
31	1051(vs)	-	1107.26	1064	11.7668	5.6191	2.3092	1.6680	bCH (73)
32	-	1035(w)	1064.46	1023	9.0674	6.2460	3.1001	2.0696	bCH (76)
33	1006(ms)	1010(ms)	1057.08	1016	37.3918	77.6774	4.8422	3.1879	bCH (77)
34	972(vs)	974(ms)	1026.46	987	4.9925	48.2117	2.1296	1.3220	bCH (75)
35	951(vw)	950(vw)	998.26	959	0.0455	0.4915	1.3070	0.7674	bCH (73)
36	943(vw)	942(vw)	979.29	941	0.0944	0.1433	1.2702	0.7177	bCC (73)
37	935(vw)	932(vw)	967.78	930	2.3035	30.2858	6.4479	3.5581	ωCH (65)
38	918(w)	920(vw)	965.98	929	1.3943	5.2078	1.4222	0.7819	ωCH (63)
39	900(vw)	903(vw)	942.49	906	1.8234	0.3785	1.3650	0.7144	ωCH (63)
40	875(ms)	-	910.33	875	1.7187	2.2893	5.5499	2.7098	ωCH (63)
41	850(vw)	853(vw)	881.03	847	0.2201	7.3782	1.4051	0.6426	ωCH (63)
42	813(vw)	815(ms)	855.31	822	0.4242	0.3257	1.4491	0.6246	ωNH(62)
43	788(vw)	-	824.99	793	5.1288	25.4328	4.8199	1.9328	ωCH (65)
44	750(vw)	-	776.49	746	22.7126	2.8729	1.8650	0.6625	ωCH (63)
45	744(vw)	-	770.40	741	28.6816	2.1012	2.8790	1.0067	ωCH (63)
46	-	730(vw)	753.40	724	66.5632	3.8225	1.8894	0.6319	R_1asymd(67)
47	-	720(vw)	746.04	717	18.2806	2.7904	1.7964	0.5891	R_1symd(65)
48	-	704(vw)	735.85	707	23.2516	3.2488	6.3630	2.0300	R_1trigd(65)

(*contd.*)

Table 3 — Vibrational assignments based on PED calculations for 2-(2-Chlorophenyl)benzimidazole (*contd.*)

S. No	Observed wave number (cm^{-1})		Wave number (cm^{-1})		IR Intensity (Km mol^{-1})	Raman activity ($Å^4$ amu^{-1})	Reduced mass (amu)	Force constant (mDyne/$Å^{-1}$)	Assignment with PED (%)
	FT-IR	FT- Raman	FT-IR	FT- Raman					
49	690(vw)	-	720.96	693	3.3305	0.5933	4.5857	1.4044	R_2asymd(67)
50	651(ms)	655(vw)	668.45	643	4.5809	11.2079	6.4124	1.6882	R_2symd(66)
51	617(ms)	-	631.19	607	1.1660	9.0949	6.5472	1.5369	R_2trigd (67)
52	561(s)	-	587.48	565	1.5300	3.6515	3.6885	0.7500	νCCl(72)
53	552(vw)	-	575.83	554	0.9280	3.3952	6.7824	1.3250	R_3asymd(67)
54	551(vw)	-	571.71	549	9.2253	0.5656	4.3817	0.8438	R_3symd(65)
55	-	499(vw)	509.83	490	7.3777	1.6745	3.3172	0.5080	R_3trigd(65)
56	457(vs)	459(vw)	471.23	453	25.5905	14.4856	2.7234	0.3563	tR_1asymd(67)
57	430(vs)	431(vw)	450.48	433	41.0153	1.4893	1.6652	0.1991	tR_1symd(65)
58	-	420(vw)	434.68	418	14.6762	6.0782	5.8366	0.6497	tR_1trigd(65)
59	-	414(vw)	432.07	415	0.5617	2.1899	2.9720	0.3269	tR_2asymd(67)
60	-	384(vw)	397.59	382	2.9835	2.0969	5.2436	0.4884	(66)$symd_2tR$
61	-	320(vw)	326.60	314	0.5034	2.3850	6.5834	0.4138	tR_2trigd (67)
62	-	274(ms)	283.10	272	0.2043	2.2747	6.0615	0.2862	tR_3asymd(67)
63	-	253(vw)	254.31	244	2.8686	10.7964	5.3005	0.2020	tR_3symd(65)
64	-	233(vw)	238.21	229	0.4520	1.8008	6.2382	0.2086	tR_3trigd(65)
65	-	171(ms)	181.61	175	0.6673	1.0702	7.3708	0.1432	ωCC(57)
66	-	151(vw)	149.85	144	0.6702	3.8954	5.7151	0.0756	bCCl(61)
67	-	88(vs)	78.89	76	0.6597	3.4996	5.3144	0.0195	ωCCl(57)
68	-	-	57.67	55	0.6671	2.8746	5.9960	0.0117	Butterfly(55)
69	-	-	29.64	28	1.2531	11.8687	5.5780	0.0029	Butterfly(55)

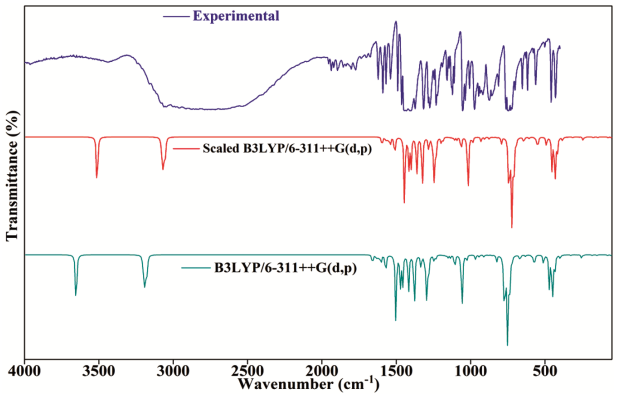

Fig. 2 — FTIR spectrum of 2-(2-Chlorophenyl)benzimidazole

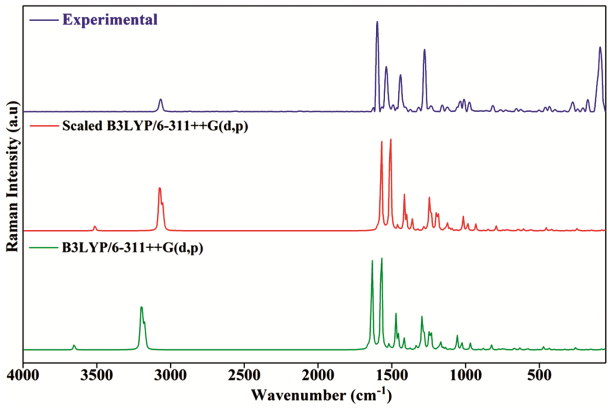

Fig. 3 — FT-Raman spectrum of 2-(2-Chlorophenyl) benzimidazole

3.2.1 N-H vibrations

Usually, the N-H stretching vibrations[30-31] creates the bands at 3500-3300 cm^{-1}. Benzomidazoles has the ability to undergo proton hopping through the protonation of nitrogen atoms and structural reorientation within a hydrogen bond network. The wide peak of the hydrogen bond indicates more favourable conditions for proton transfer since it symbolizes the energy needed to support the imidazole ring's resonance structure and the change from a covalent link (N–H) to a hydrogen bond (N···H). In this case, the broad band seen at 3520 cm^{-1} is recognized as the N-H stretching vibration of CPBZ. The N-H stretching mode is identified with a computed wave number of 3511 cm^{-1} using the B3LYP technique. The fact that the PED column makes up 99% of the mode indicates that it is pure. Further, the scaled band at 1187 cm^{-1} with 72% PED and the N-H in-plane bending vibrations that were seen in the FTIR at 1185 cm^{-1} are in excellent agreement. For the N-H out-of-plane bending vibration, the scaled frequencies calculated in the 822 cm^{-1} range are in agreement with the experimental values obtained in FTIR at 813 cm^{-1} and FT-Raman at 815 cm^{-1} (62% PED).

3.2.2 C-H vibrations

The experimental spectra of aromatic compounds contain the C-H stretching frequencies, C-H in-plane bending vibrations, and C-H out-of-plane bending vibrations[32] in the ranges of 3100–3000 cm^{-1}, 1300-1000 cm^{-1}, and 1000–750 cm^{-1}, respectively[33]. The vibrational frequencies detected between 3081-3040 cm^{-1} and 3067 cm^{-1} in the FTIR and FT-Raman spectra, respectively, are consistent with the B3LYP/6-311++G(d,p) technique and are attributed to C–H stretching vibrations (92–98% PED). The FT-IR and FT-Raman bands between 1126–951 cm^{-1} and 1122–950 cm^{-1}, respectively, (73–76% PED) are in good agreement with the scaled C-H in-plane bending vibrations, which were computed in the 1125–959 cm^{-1} range. The scaled frequencies, which fall between 930 and 741 cm^{-1} (62–65% PED) for the C-H out-of-plane bending vibrations, match the experimental values discovered in FTIR between 935-744 cm^{-1} and FT-Raman between 932 and 853 cm^{-1}.

3.2.3 C-N vibrations

Since mixing of many bands is possible in the composite area of the vibrational spectrum where the C-N stretching frequency occurs[34], the range 1386–1266 cm^{-1} was assigned to the aromatic molecule's C-N stretching absorption. The bands with PED contributions of 74, 72, and 69%, respectively, at 1591, 1568, and 1537 cm^{-1} in FT-IR and 1598, 1566, and 1537 cm^{-1} in FT-Raman have been recognized as C-N stretching vibrations. The bands seen at 1620 cm^{-1} in FT-IR and 1624 cm^{-1} in FT-Raman are classified as C=N stretching vibrations (74% PED), whereas the theoretically scaled wavenumbers obtained at 1571, 1557, and 1541 cm^{-1} are assigned as C-N stretching vibrations.

3.2.4 C-C vibrations

The region between 1650 and 1400 cm^{-1} is frequently where the ring carbon-carbon C-C stretching vibrations for hetero aromatic compounds are seen[35]. The FTIR at 1489, 1373, 1315, 1276, 1248, and 1226 cm^{-1} and the FT-Raman at 1515, 1450, 1441, 1420, 1400, 1350, 1317, 1278, 1251, 1241, 1200, and 1158 cm^{-1} (80-85% PED) have detected the C-C stretching vibrations. These results are consistent with scaled values between the ranges 1511-1141 cm^{-1}. The theoretically predicted C-C in-plane bending frequencies at 941 cm^{-1} are in good agreement with those observed in the actual FTIR and FT-Raman spectra at 943 cm^{-1} and 942 cm^{-1} (73% PED), respectively. Similar to this, there is a good agreement between the experimentally obtained C-C out-of-plane bending[36] Raman frequency, which was discovered at 171 cm^{-1} (57% PED), and the theoretically expected value, which was calculated at 175 cm^{-1} at scaled B3LYP level. Furthermore, Table 3 presents illustrations of the CPBZ ring modes of vibration.

3.2.5 C-Cl vibrations

The C-Cl vibrations[37] usually occur in the range of 850 and 550 cm^{-1}. Consequently, the FTIR peak absorbed at 561 cm^{-1} (72% PED) and the calculated wavenumber at 565 cm^{-1} has been ascribed to the stretching C-Cl vibration of CPBZ. For most chloro aromatic compounds, the band with different intensities in the range 385-265 cm^{-1} has been called the C-Cl bending in-plane vibration[38]. As a result, the C-Cl in-plane deformation for CPBZ has selected the Raman peak at 151 cm^{-1}. A strong Raman peak has been identified for the out-of-plane C-Cl deformation of CPBZ at 88 cm^{-1}.

3.3 Frontier Molecular Orbitals

The border orbitals with the highest occupied (HOMO) and lowest unoccupied (LUMO) energies have a major impact on characteristics related to charge transfer, electrical conductivity, and absorption. Quantum chemistry metrics such border orbital gap, HOMO, and LUMO are used to illustrate the molecules' kinetic stability and chemical reactivity[39]. At B3LYP/6-311++G(d,p) in CPBZ, the orbital energy gap and HOMO and LUMO energies were measured. Fig. 4 displays the CPBZ boundary orbitals in three dimensions. The ionization energy

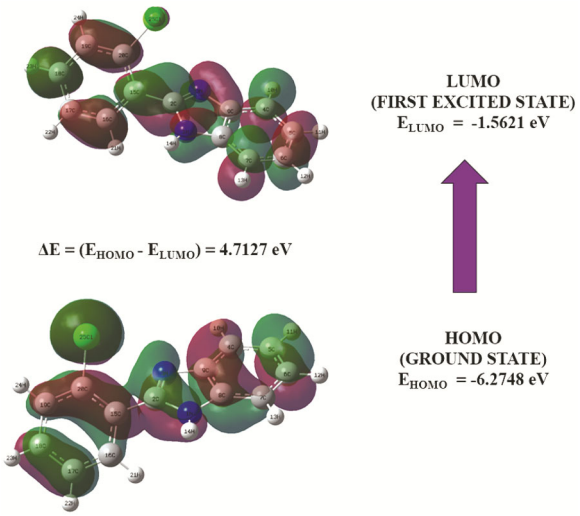

Fig. 4 — HOMO-LUMO plot of 2-(2-Chlorophenyl) benzimidazole

and electron affinity are found using the HOMO and LUMO energies, respectively, as $I = -E_{HOMO}$ and $A = -E_{LUMO}$. Hard molecules are identified by a broad HOMO-LUMO gap and are linked to more stable compounds, whereas soft molecules are identified by a small gap and are linked to more reactive molecules[40].

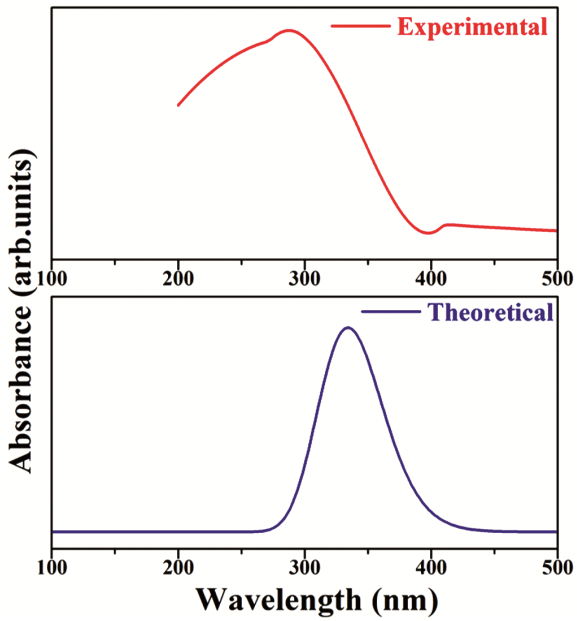

Fig. 5 — UV plot of 2-(2-Chlorophenyl)benzimidazole

Table 4 — Global reactivity descriptors for 2-(2-Chlorophenyl)benzimidazole

Molecular Properties	B3LYP/6-311++G(d,p)
HOMO (eV)	-6.2748
LUMO (eV)	-1.5621
ΔE (E_{HOMO} -E_{LUMO}) (eV)	4.7127
Ionization potential (I) (eV)	6.2748
Electron affinity (A) (eV)	1.5621
Global hardness (η) (eV)	2.3563
Global softness (s) (eV^{-1})	0.2122
Electronegativity (χ) (eV)	3.9185
Chemical potential (μ) (eV)	-3.9185
Global electrophilicity (w) (eV)	3.2580

Based on calculations, the HOMO energy of CPBZ is found to be -6.2748 eV, meaning that the ring's chlorine atom can act as the electron donor. Predicted LUMO values of -1.5621 eV show that the ring's C-C bond functions as the primary electron acceptor, and an energy gap of 4.7127 eV is determined. Table 4 presents significant global reactivity attributes for CPBZ, which were determined by the use of the B3LYP/6-311++G(d,p) approach, which is grounded in Koopman's relations[41]. The stability order of molecular systems is verified using the definition of electronegativity (χ), which is the opposite of chemical potential. Chemical hardness is a good indicator of chemical stability[42]. It is determined that the gas phase chemical hardness and softness of CPBZ are 2.3563 eV and 0.2122 eV^{-1}, respectively. The computed values for CPBZ's chemical potential and global electrophilicity are -3.9185 eV and 3.2580 eV, respectively.

3.4 UV-Vis Spectra Analysis

The electronic transitions of CPBZ were investigated using the time-dependent TD-DFT/B3LYP/6-311++G(d,p). A crucial element of TD-DFT, a helpful technique for analyzing the static and dynamic properties of molecules in their excited states, is the configuration interaction between singly excited electronic states[43–44]. The UV spectra obtained from theoretical and practical approaches are shown in Fig. 5. The calculated oscillator power, wavelength (k), spectrum allocations, and excitation energies are listed in Table 5. Experimentation revealed that the maximum absorption value in methanol is 292.31 nm. As a consequence, the calculated electronic transitions at 352.04 nm agree with the observed result, indicating the largest H-2→L contribution of 93%. The apparent peak in the spectrum is caused by the π→π* transition, which happens when electron density moves from a lone pair of electrons located on electronegative components like the nitrogen and chlorine atoms in the CPBZ molecule to the electrons of the phenyl ring.

Table 5 — Molecular orbital contributions of 2-(2-Chlorophenyl)benzimidazole

TD-DFT/ B3LYP/6-311++G(d,p)

Energy(eV)	Oscillator strength	Computed wavelength (nm)	Experimental wavelength(nm)	Major contributions	Assignment
2.7077	0.0000	457.90	-	H→L (87.57 %)	π→π*
3.4424	0.0000	360.17	-	H-1→L (66.26 %)	π→π*
3.5218	0.0000	352.04	292.31	H-2→L (93.13 %)	π→π*

3.5 DOS Spectra and NBO Analysis

It is possible for neighbouring orbitals in a border zone to have the same degenerate energy levels. If so, using HOMO and LUMO alone to characterize border orbitals may not be appropriate. Because of this, overlap population density of states (OPDOS), also called crystal orbital overlapping population (COOP-Crystal Orbital Overlapping Population), is a composite of alpha (α) and beta (β) electron densities of states[45–46] that are created by utilizing the GaussSum 3.0 program to integrate molecular orbital data with Gaussian curves. Fig. 6 illustrates how an orbital configuration of a molecule affects its chemical bonding in CPBZ. The density of state plot is used to show the composition of the energy gap and border orbitals of the system. PDOS illustrates how certain atoms or functional groups contribute to each molecular orbital. We might use relevant components to assess non-bonding, bonding, and anti-bonding qualities using OPDOS[47]. On OPDOS graphs, positive values indicate bonding interactions, negative values indicate anti-bonding interactions, and values around zero indicate non-bonding interactions. A total of 118 electrons occupy the DOS of CPBZ, which consists of both 59α and 59β electrons. In the CPBZ structure, interactions between chlorine and nitrogen and hydrogen atoms show anti-bonding, whereas interactions between chlorine and carbon atoms and nitrogen and hydrogen atoms show bonding, as can be seen in the COOP diagram (Fig. 6). NBO studies offer in-depth understanding of intra- and intermolecular bonding interactions inside the molecule[48]. It offers a clear understanding of the relationships between the linkages. Table 6 reports the results of the DFT/B3LYP/6-311++G(d,p) calculation for NBO investigation. These results are utilized to analyze the delocalization interactions, the donor and acceptor orbitals, and the stabilization energy. A big stabilization energy value indicates a significant interaction between donors and acceptors. This suggests a greater degree of conjugation as well as a greater propensity on the part of electron donors to give more to acceptors.

ED (i) and ED (j) reflect the stabilizing donor and acceptor interaction over the bound atom. While an empty or full bonding, an anti-bonding, or a lone pair can be a donor, a filled bonding or a lone pair can be an acceptor. These exchanges are necessary for a solid connection. The connection will be strengthened if the contact is part of a bonding pair; on the other hand, the

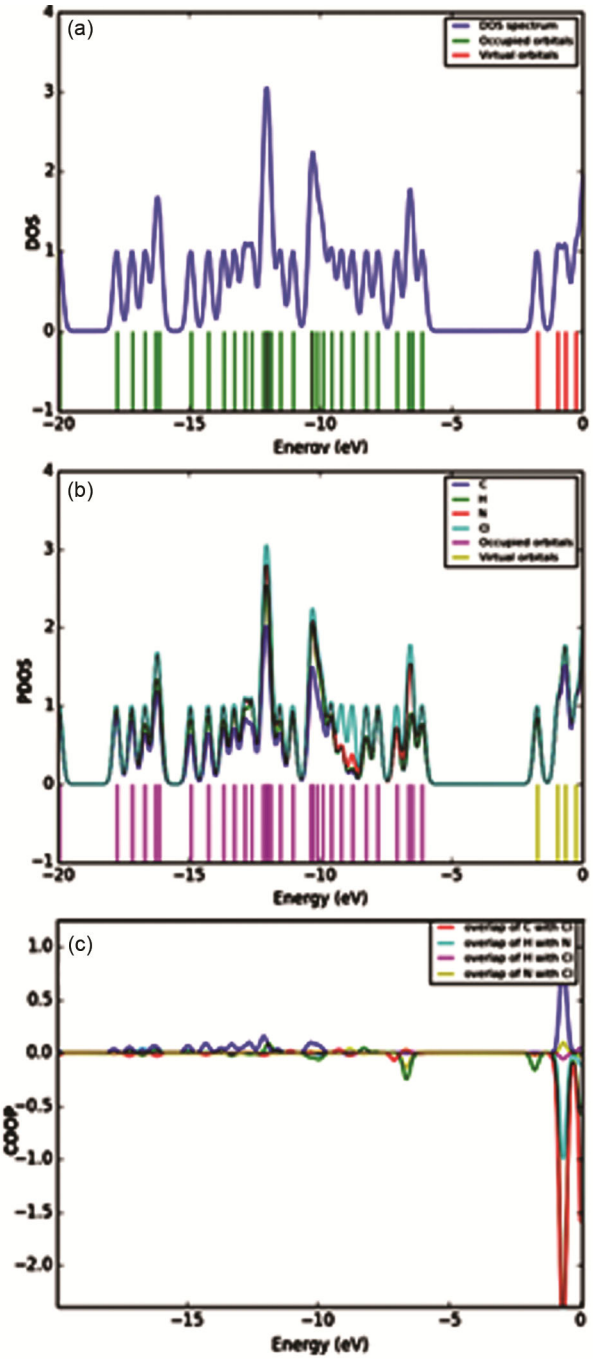

Fig. 6 — (a) DOS (b) PDOS (c) COOP Spectra of 2-(2-Chlorophenyl)benzimidazole

bond will be diminished if a single pair acts as the donor or acceptor[49]. The molecule is unique for biological reasons because of its increased stabilization energy between the π and π* orbitals. In CPBZ, the lone pair LP(1) of the N1 atom was transferred to the anti-bonding orbital π*(C2-N3), displaying a stabilization energy of 23.73 kcal/mol. But N1 and N3

Table 6 — Second-order perturbation theory analysis of Fock matrix for 2-(2-Chlorophenyl)benzimidazole

Donor(i)	ED (i) (e)	Acceptor (j)	ED (j) (e)	Stabilization energy E(2) (Kcal/mol)	Energy difference E (j) −E (i) (arb. units)	Fock matrix element F(i,j) (arb. units)
π(C2-N3)	0.9261	LP*(1)C9	0.5064	15.6	0.18	0.089
π(C2-N3)	0.9261	π*(C15-C16)	0.1952	3.89	0.31	0.047
σ(C4-C5)	0.9871	σ*(N3-C9)	0.0132	3.46	1.08	0.077
π(C4-C5)	0.8412	LP*(1)C9	0.5064	26.15	0.14	0.095
π(C4-C5)	0.8412	π*(C6-C7)	0.1838	10.59	0.27	0.069
σ(C6-C7)	0.9851	σ*(N1-C8)	0.0134	3.8	1.03	0.079
π(C6-C7)	0.8456	π*(C4-C5)	0.1696	9.77	0.28	0.067
π(C15-C16)	0.8271	π*(C2-N3)	0.1831	8.25	0.26	0.059
π(C15-C16)	0.8271	π*(C17-C18)	0.1705	9.58	0.29	0.066
π(C17-C18)	0.8246	π*(C15-C16)	0.1952	11.26	0.29	0.073
π(C19-C20)	0.9895	π*(C15-C16)	0.1952	10.12	0.3	0.07
π(C19-C20)	0.9895	π*(C17-C18)	0.1705	9.64	0.29	0.067
σ(C20-Cl25)	0.9931	σ*(C18-H23)	0.0066	3.75	2.16	0.114
σ(C20-Cl25)	0.9931	σ*(C19-H24)	0.0066	3.4	2.16	0.108
LP(1) N1	0.8223	π*(C2-N3)	0.1831	23.73	0.26	0.099
LP(1) N3	0.9686	σ*(N1-C2)	0.0160	3.36	0.77	0.065
LP(1) C8	0.5150	LP*(1)C9	0.5064	652.05	0.02	0.128
LP(1) C8	0.5150	π*(C6-C7)	0.1838	33.73	0.15	0.107
LP*(1) C9	0.5064	π*(C2-N3)	0.1831	24.64	0.09	0.071
LP*(1) C9	0.5064	π*(C4-C5)	0.1696	36.19	0.14	0.109
π(C2-N3)	0.1831	π*(C15-C16)	0.1952	24.31	0.04	0.063

atoms' lone pair transition through the LP(1) of C8 and C9 atoms to π*(C6-C7) and π*(C4-C5) showed a notable stabilizing energy of 33.73 and 36.19 kcal/mol. The significant delocalization is demonstrated by the strong interaction between the anti-lone pair bonding orbital LP*(1) of the C9 atom, which has an energy of 652.05 kcal/mol, and the LP(1) orbital of the C8 atom. The variables that significantly affect the CPBZ molecule's stability are listed in Table 6.

3.6 Mulliken Charge Analyses

Research on Mulliken charges has a dynamic function in the chemical system because of its connections to electronic charges and dipole moment[50]. Quantum theory is dynamically used in the case of reactive charges, which influence the electrical properties of the molecule. The exchange and balancing of electronegativity in chemical processes[51] to external molecule surfaces has also been described in terms of the Mullikan charge. Table 7 contains the Mulliken charges for CPBZ utilizing B3LYP and 6-311++G(d,p) basis set. H10, H11, H12, H13, H14, H21, H22, H23, and H24 are all positive values, indicating that CPBZ has a higher acidity (0.1828, 0.1673, 0.1655, 0.1474, 0.3093, 0.0557, 0.1912, 0.1615, and 0.2102). N1 and N3, the nitrogen atoms, are charged with -0.1655 and 0.1705, respectively. The charges of both positive and

Table 7 — Mulliken atomic charge for 2-(2-Chlorophenyl)benzimidazole

Atoms	Atomic Charges (Mulliken) B3LYP/6-311++G(d,p)
N1	-0.1655
C2	-0.7363
N3	0.1705
C4	-0.3776
C5	-0.2686
C6	-0.3425
C7	-0.5575
C8	0.9066
C9	0.2035
H10	0.1828
H11	0.1673
H12	0.1655
H13	0.1474
H14	0.3093
C15	0.2918
C16	-0.3950
C17	-0.3795
C18	-0.4204
C19	-0.4338
C20	0.4555
H21	0.0557
H22	0.1912
H23	0.1615
H24	0.2102
C125	0.4580

negative carbon atoms (C2, C4, C5, C6, C7, C8, C9, C15, C16, C17, C18, C19, and C20) are significantly affected by substituents. Moreover, the two charges of carbon (C8 and C2) atoms represent the largest positive and negative charges in CPBZ (0.9066 and -0.7363), while the positive charge on the chlorine atom (Cl25) is 0.4580.

3.7 Fukui Function

In computational chemistry based on Mulliken population analysis, the Fukui function is used to quantify the electrophilicity and nucleophilicity of each atom[52–53]. Mulliken population analysis is used to obtain the individual charges of the Fukui function. The Fukui functions are defined by the following expression, which provides the CPBZ's reactivity.

$$f_k^+ = q_j(N+1) - q_j(N)$$

$$f_k^- = q_j(N) - q_j(N-1)$$

$$f_k^0 = \frac{1}{2}[q_j(N+1) - q_j(N-1)] \quad \ldots (1)$$

Here, free radical, electrophilic, and nucleophilic interactions are applied to the reference molecule. where q_j represents the atomic charge at the jth atomic site and N, N+1, and N-1 are the neutral, anionic, and cationic chemical species. A dual descriptor was recently presented by Morell *et al.*[54], and the equation is as follows:

$$\Delta f(r) = f_k^+ - f_k^- \quad \ldots (2)$$

Each atom's dual descriptor value is explained by the dual descriptor, which makes a distinction between electrophilic and nucleophilic functions that attack at a certain location and sign. The nucleophilic sites for CPBZ in this study include C2, C4, C5, C6, C7, H13, H14, C16, C17, C18, C19, and H21, which meet the requirements of the dual descriptor based on the values displayed in Table 8. Conversely, electrophilic sites with negative values are found in N1, N3, C8, C9, H10, H11, H12, C15, C20, H22, H23, H24, and Cl25. During the process, the local behaviour of the molecule CPBZ controls its response to both nucleophilic and electrophilic attack.

3.8 MEP Analysis

In biochemistry, MEP mapping combined with DFT techniques might be helpful in figuring out drug-receptor interactions. The MEP, which is connected to a molecule's chemically active regions, increases awareness of molecular reactivity, substituent effects,

Table 8 — Fukui functions from Mulliken charges for 2-(2-Chlorophenyl)benzimidazole

Atoms	Mulliken Charges			Fukui functions			
	q(N+1)	q(N)	q(N-1)	f_k^+	f_k^-	f_k^0	$\Delta f(r)$
N1	-0.8685	-0.1655	-0.8393	-0.7030	0.6738	-0.0146	-1.3768
C2	0.3581	-0.7363	0.4541	1.0944	-1.1904	-0.0480	2.2848
N3	-0.5033	0.1705	-0.3808	-0.6738	0.5512	-0.0613	-1.2250
C4	-0.1100	-0.3776	0.0094	0.2676	-0.3870	-0.0597	0.6546
C5	-0.1654	-0.2686	-0.1436	0.1032	-0.1249	-0.0109	0.2281
C6	-0.1914	-0.3425	-0.1128	0.1511	-0.2297	-0.0393	0.3808
C7	-0.0959	-0.5575	-0.0080	0.4616	-0.5496	-0.0440	1.0112
C8	0.2422	0.9066	0.2767	-0.6644	0.6299	-0.0173	-1.2943
C9	-0.0081	0.2035	-0.0070	-0.2116	0.2105	-0.0005	-0.4221
H10	0.1178	0.1828	0.2301	-0.0649	-0.0473	-0.0561	-0.0176
H11	0.0949	0.1673	0.2107	-0.0724	-0.0434	-0.0579	-0.0290
H12	0.0909	0.1655	0.2157	-0.0746	-0.0502	-0.0624	-0.0244
H13	0.1073	0.1474	0.2167	-0.0402	-0.0693	-0.0547	0.0292
H14	0.3002	0.3093	0.3874	-0.0091	-0.0782	-0.0436	0.0691
C15	0.0849	0.2918	0.1148	-0.2068	0.1770	-0.0149	-0.3838
C16	-0.0910	-0.3950	-0.0185	0.3040	-0.3765	-0.0363	0.6805
C17	-0.2026	-0.3795	-0.1795	0.1769	-0.2000	-0.0116	0.3770
C18	-0.1536	-0.4204	-0.0546	0.2669	-0.3658	-0.0495	0.6327
C19	-0.1102	-0.4338	-0.0770	0.3236	-0.3568	-0.0166	0.6804
C20	-0.2934	0.4555	-0.2715	-0.7489	0.7270	-0.0109	-1.4759
H21	0.0962	0.0557	0.1757	0.0404	-0.1200	-0.0398	0.1604
H22	0.0943	0.1912	0.2017	-0.0969	-0.0105	-0.0537	-0.0864
H23	0.0930	0.1615	0.2115	-0.0685	-0.0501	-0.0593	-0.0184
H24	0.1183	0.2102	0.2210	-0.0919	-0.0108	-0.0514	-0.0812
Cl25	-0.0046	0.4580	0.1671	-0.4626	0.2909	-0.0858	-0.7536

electrophilic reactions, and intra- and intramolecular connections[55]. The reactive sites of the molecule are identified by MEP in terms of colours[56–57]. Fig. 7 shows the CPBZ MEP schematic. The colour red represents the most advantageous location for an electrophilic site, whereas the colour blue represents the most advantageous zone for a nucleophilic site. This chemical is more electrophilic at the location surrounding the nitrogen atom (N3), as indicated by the red area. The hydrogen (H14 and H21) atoms of the molecule are located in the blue nucleophilic region. As a result, the chemical's reactive areas, which are easily identified using information on electron and proton interactions, may exhibit biological activity. While the positive electrostatic potential (ESP) is focused over the rest section of the molecule, the negative electrostatic potential (ESP) is seen as a yellowish blob over the nitrogen and chlorine atoms.

3.9 NMR Analysis

NMR spectroscopy is one of the most important techniques for examining the structural conformation of organic compounds. The number of various protons as well as the makeup of each proton's immediate surrounds may be determined from the 1H NMR spectrum. The 13C NMR spectrum also provides structural information on the different carbon atoms that are present in the molecule, which may be used to understand more about the molecule under study. The GIAO approach is used to predict the theoretical 13C and 1H chemical shifts[58-59] in order to determine the ideal geometry from B3LYP/6-311++G(d,p). Theoretical values for CPBZ's proton (1H) and carbon (13C) NMR chemical shifts are listed in Table 9. Thirteen carbon atoms and nine hydrogen atoms make up the CPBZ molecule. Table 9 indicates that, on average, the carbon (13C) NMR chemical shifts of an organic molecule vary from 60 to 62 ppm. The study determined that the 1H NMR theoretical chemical shift of the CPBZ molecule ranged from 7.53 to 10.41 ppm, and that the aromatic carbons in the molecule ranged from 115.18 to 175.73 ppm.

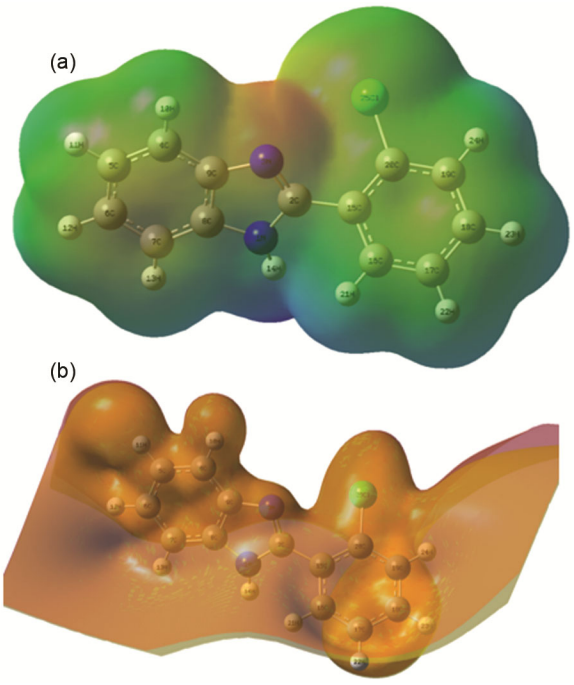

Fig. 7 — (a) MEP and (b) ESP plot for 2-(2-Chlorophenyl) benzimidazole

3.10 Cytotoxicity Analysis

The MCF-7 breast cancer cell line was used to assess CPBZ's anti-cancer efficacy. For this, live MCF-7 cells were extracted and counted using a hemocytometer. After that, they were divided across separate 96-well plates after being diluted with DMEM medium. After that, the cells were grown for a whole day in order to promote adhesion[60]. Following their insertion into each well, the MCF-7 cells were treated to several doses of CPBZ (5–20 µg/ml) as well as a control. The proportion of stable cells relative to the control was used to express the results. Following treatment with sample CPBZ, MCF-7 cells exhibit contraction, detachment, blebbing, and deformed shape, as seen in the photomicrograph (20x). Control is in opposition to these developments. When control cells were seen

Table 9 — ^{13}C and ^{1}H NMR chemical shifts for 2-(2-Chlorophenyl)benzimidazole

^{13}C Assignment	Calculated Shift (ppm)	^{1}H Assignment	Calculated shift (ppm)
C7	115.18	H22	7.53
C4	122.80	H12	7.60
C16	127.5	H23	7.63
C6	127.61	H13	7.66
C5	128.60	H11	7.74
C17	131.21	H24	7.88
C18	134.97	H21	7.90
C15	134.97	H10	8.27
C19	138.15	H14	10.41
C8	151.66		
C20	152.06		
C9	159.48		
C2	175.73		

under a light microscope, they revealed their typical, undamaged morphology. The morphological alterations and percentage of cell survival seen in breast cancer MCF-7 cells at different doses after exposure to CPBZ are displayed in Fig. 8. A comparison was made between the half maximum inhibitory concentrations (IC50) values and the optimal dosages at different periods.

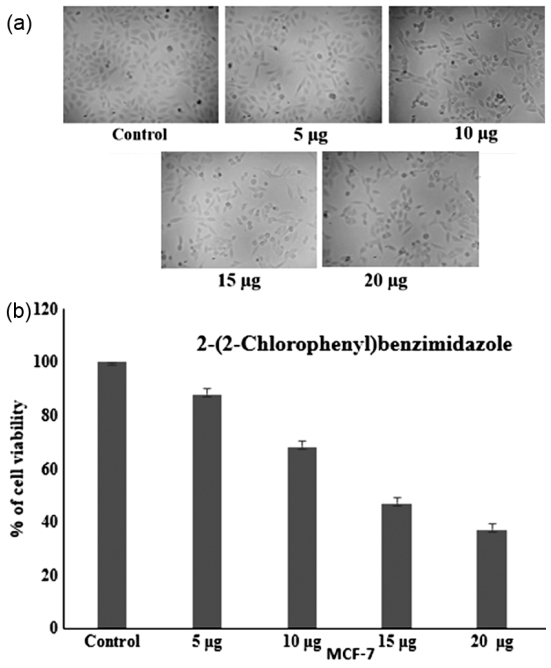

Fig. 8 — (a) Morphological changes (b) % of cell viability for different concentrations of 2-(2-Chlorophenyl)benzimidazole against breast cancer MCF-7 cells

When the dose-dependent approach was used to get the IC50 values, the result was a 50% reduction in cytotoxicity when compared to control cells. Every experiment was repeated at least three times. Because of its low IC50 value, the sample CPBZ exhibited remarkable activity against the breast cancer cell line MCF-7. It is determined that the IC50 value for CPBZ with MCF-7 is 15.53 µg/ml.

3.11 Antibacterial Activity

The antibacterial activity were performed using both Gram-positive and Gram-negative bacteria, including Escherichia coli, Serratia, and Klebsiella, as well as Methicillin-Resistant Staphylococcus aureus (MRSA) and Vancomycin-Resistant Enterococcus faecium (VREF) cultures. According to data, the CPBZ chemical can restrict the metabolic growth of the bacteria under investigation, especially Klebsiella, as seen in Fig. 9. It would be logical to anticipate that a much greater proportion of drugs will target gram-positive bacteria than gram-negative germs when assessing whether a drug's antibacterial effect is gram-positive or gram-negative[61]. The remarkable activity of this molecule has been shown to be attributed to the benzimidazole ring, which may play a critical role in its antibacterial action[62]. It has been shown that CPBZ is a very potent anti-Klebsiella agent since its inhibition zones expand with concentration. Therefore, in terms of the zone of inhibition, the E. Coli, MRSA, VREC, and Serratia are inactive (Table 10 and Fig. 9).

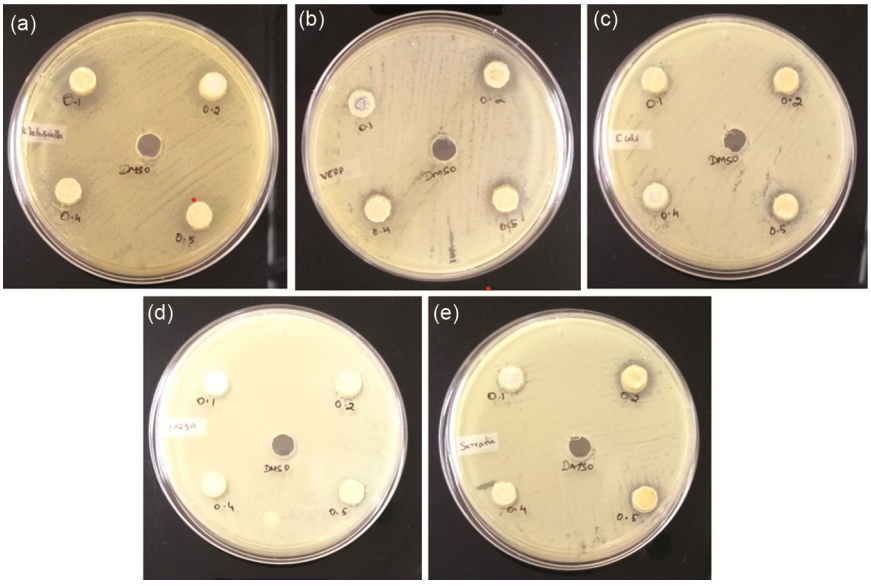

Fig. 9 — Inhibition zone representation of different bacteria treated with 2-(2-Chlorophenyl)benzimidazole: (a) Klesiella, (b) Vempicillin Resistant Escheria coli (c) E. Coil (d) Multidrug Resistance Staphylococcus aureus, and (e) Serratia

Table 10 — Antibacterial analysis of 2-(2-Chlorophenyl)benzimidazole with various bacteria

2-(2-Chlorophenyl)benzimidazole Concentration (µg/mL)	Zone of Inhibition (mm)				
	Escherichia coli	Methicillin-resistant Staphylococcus aureus	Vempicillin Resistant Escheria coli	Serratia	Klebsiella
0.1	0	0	0	0	1
0.2	0	0	0	0	2
0.4	0	0	0	0	3
0.5	0	0	0	0	5

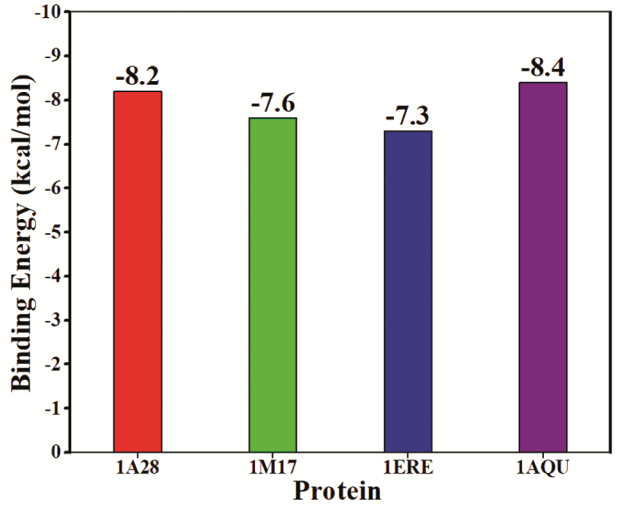

Fig. 10 — Comparison of binding energy of 2-(2-Chlorophenyl)benzimidazole with 1A28, 1M17, 1ERE and 1AQU

3.12 Molecular Docking Analysis

Molecular docking predicts the active site residues and schematic binding process between proteins and small molecule ligands[63]. Drug development uses a computer approach called molecular docking to look at the binding sites of proteins and ligands[64–65]. The human progesterone receptor (PDB ID: 1A28), the epidermal growth factor receptor (PDB ID: 1M17), the human estrogen receptor (PDB ID: 1ERE), and the estrogen sulfotransferase receptor (PDB ID: 1AQU) are among the proteins that CPBZ interacts with, according to our in-silico research (Figs. 10 & 11). Table 11 shows the binding energies for various proteins. Our results show that the protein 1AQU and CPBZ have the greatest interaction with the H-bonding residues THR A:227 and LYS A:197, with a calculated binding free energy of -8.4 kcal mol^{-1}. Additionally, the present study found that, with a binding energy of -8.2 $kcalmol^{-1}$, CPBZ has a higher affinity for protein 1A28 at MET A:756. With regard to the other breast cancer proteins 1M17 and 1ERE, CPBZ exhibited noteworthy binding free energies of -7.6 and -7.3 $kcalmol^{-1}$, respectively. The conclusion

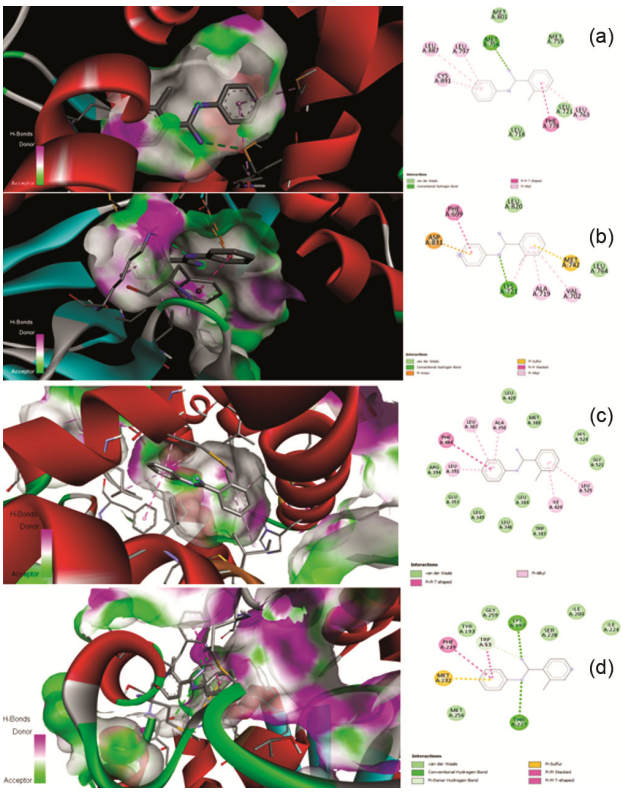

Fig. 11 — Interaction of 2-(2-Chlorophenyl)benzimidazole with (a) 1A28 (b) 1M17 (c) 1ERE and (d) 1AQU

that CPBZ had the strongest anti-breast cancer effect seems sense.

3.13. ADMET Prediction

The appropriateness of CPBZ for human use has been determined by testing its ADMET properties, which include skin permeability, LD50, P-glycoprotein inhibition, Blood Brain Barrier (BBB), and Human Intestinal Absorption (HIA). The BBB value of the CPBZ molecule was found to be 0.309, suggesting that it has less harmful effects on the central nervous system[66,67]. Projected parameters were important and helpful in selecting orally bioactive chemicals and moving the therapy candidate to the next step since CPBZ has a Human Intestinal Absorption[68] (HIA) value of 93.175%. When

Table 11 — Comparison of binding energy of 2-(2-Chlorophenyl)benzimidazole with 1A28, 1M17, 1ERE and 1AQU along with interacting residues

S. No	Protein	Binding Energy (kcal/mol)	Interacted Residues	Ligand and Protein atom involved in H-bonding
1	Human Progesterone Receptor (1A28)	-8.2	MET A:756,MET A:801,MET A:759, LEU A:721,LEU A:763,PHE A:778,LEU A:718, LEU A:797,LEU A:887,CYS A:891	MET A:756
2	Epidermal Growth Factor Receptor (1M17)	-7.6	LYS A:721,ASP A:831,PHE A:699, LEU A:820,MET A:742,LEU A:764,VAL A:702, ALA A:719	LYS A:721
3	Human Estrogen Receptor (1ERE)	-7.3	LEU A:525,ILE A:424,ALA A:350,LEU A:387,PHE A:404,LEU A:391,ARG A:394,GLU A:353,LEU A:349,LEU A:346,LEU A:384,TRP A:383,LEU A:428,MET A:388,HIS A:524,GLY A:521	_
4	Estrogen Sulfotransferase Receptor (1AQU)	-8.4	THR A:227,LYS A:197,PHE A:229,TRP A:53,MET A:232,MET A:256,TYR A:193,GLY A:259,SER A:228,ILE A:200,ILE A:224	THR A:227,LYS A:197

Table 12 — ADMET profile of 2-(2-Chlorophenyl)benzimidazole

ADMET prediction	Value	ADMET prediction	Value
CaCo-2 permeability (log Papp in 10^{-6}cm/s)	1.508	P-glycoprotein substrate	No
Intestinal absorption (human) (%)	93.175	P-glycoprotein I inhibitor	No
Skin Permeability (log Kp)	-2.046	P-glycoprotein II inhibitor	No
VDss (human) (log L/kg)	0.503	Total Clearance (log ml/min/kg)	0.439
Fraction unbound (human) (Fu)	0.327	Renal OCT2 substrate	No
BBB permeability (log BB)	0.309	AMES toxicity test	No
CNS permeability (log PS)	-2.503	Max. tolerated dose (human) (log mg/kg/day)	0.071
CYP2D6 substrate	No	hERG I inhibitor	No
CYP3A4 substrate	No	hERG II inhibitor	No
CYP1A2 inhibitior	Yes	Oral Rat Acute Toxicity (LD50) (mol/kg)	2.668
CYP2C19 inhibitior	No	Oral Rat Chronic Toxicity (LOAEL) (log mg/kg_bw/day)	0.904
CYP2C9 inhibitior	No	Hepatotoxicity	No
CYP2D6 inhibitior	No	Skin Sensitisation	No
CYP3A4 inhibitior	No	T.Pyriformis toxicity (log ug/L)	1.931
Carcinogenicity	non	Minnow toxicity (log mM)	1.526

predicting human poisoning symptoms after an acute overdose, the LD50 is crucial. For sample CPBZ, the lowest LD50 value was 2.668 mol/kg. Moreover, several ADMET parameters were discovered and are displayed in Table 12. These results indicate that CPBZ has a high plasma protein binding, a positive blood brain barrier bridging, and a reasonable chance of intestinal absorption in people.

4 Conclusions

The present investigation has employed vibrational frequency (FTIR, FT-Raman), quantum chemistry computations, and molecular structure analysis to ascertain the structural and spectroscopic properties of 2-(2-Chlorophenyl) benzimidazole. The molecule was studied theoretically using B3LYP functional with 6-311++G (d,p) level of theory. The experimental XRD, FTIR, and FT-Raman data are compared with the optimized geometry and frequency. The calculated HOMO-LUMO and global reactivity descriptors exhibit an energy gap of 4.7127 eV, indicating that interatomic interactions are the source of the charge transfer. The result of NBO shows that $\pi \rightarrow \pi^*$ electron delocalization causes intra- and intermolecular charge exchange. The electrophilic assaults over the nitrogen atoms and the nucleophilic attacks on the hydrogen

atoms are demonstrated by the MEP and Mulliken studies. The molecule's carbon and proton NMR shifts have been computed. Docking studies indicate that CPBZ has a high binding energy of -8.4 kcal/mol with the interaction of estrogen sulfotransferase receptor (PDB ID: 1AQU). Based on its cytotoxicity, docking, and ADMET findings, CPBZ will thus be a powerful anti-breast cancer medication with minimal adverse effects during medical procedures.

Acknowledgments

The authors would like to thank the management of Kalasalingam Academy of Research and Education, for providing the financial support to establish the computational research facility at the International Research Centre (IRC), Kalasalingam Academy of Research and Education.

References

1 Farmanzadeh D & Najafi M, *J Theor Comput Chem*, 14 (2015) 1550018.
2 Song M, Yang F, Liu L, Shen L, Hu P, Zhang L & Su C, *Spectrochim Acta A Mol Biomol Spectrosc*, 196 (2018) 49.
3 Bouchouit M, Said M E, Kara Ali M, Bouacida S, Merazig H, Kacem Chaouche N, Chibani A, Zouchoune B, Belfaitah A & Bouraiou A, *Polyhedron*, 119 (2016) 248.
4 Veerasamy R, Roy A, Karunakaran R & Rajak H, *Pharmaceuticals*, 14 (2021) 663.
5 Chen G, Liu Z, Zhang Y, Shan X, Jiang L, Zhao Y, He W, Feng Z, Yang S & Liang G, *ACS Med Chem Lett*, 4 (2012) 69.
6 Tonelli M, Simone M, Tasso B, Novelli F, Boido V, Sparatore F, Paglietti G, Pricl S, Giliberti G, Blois S, Ibba C, Sanna G, Loddo R & La Colla P, *Bioorg Med Chem*, 18 (2010) 2937.
7 Şahin E, İde S, Kurt M & Yurdakul Ş, *J Mol Struct*, 616 (2002) 259.
8 Nath J, Paul R, Ghosh S K, Paul J, Singha B & Debnath N, *Life Sci*, 258 (2020) 118189.
9 Song B, Park E Y, Kim K J & Ki S H, *Cancers*, 14 (2022) 4601.
10 Nguyen V T, Huynh T K C, Ho G T T, Nguyen T H A, Le Anh Nguyen T, Dao D Q, Mai T V T, Huynh L K & Hoang T K D, *R Soc Open Sci*, 9 (2022) 220659.
11 Haider K & Yar M S, *Advances of Benzimidazole Derivatives as Anticancer Agents: Bench to Bedside*, IntechOpen Ltd, London, 2022.
12 Venugopal S, Kaur B, Verma A, Wadhwa P, Magan M, Hudda S & Kakoty V, *Chem Biol Drug Des*, 102 (2023) 357.
13 Lee Y T, Tan Y J & Oon C E, *Acta Pharmaceutica Sinica B*, 13 (2023) 478.
14 Murugan P, Jeyavijayan S, Ramuthai M & Narmadha R B, *Polycycl Aromat Compd*, 43 (2022) 2889.
15 Xavier T S, Rashid N & Hubert Joe I, *Spectrochim Acta A Mol Biomol Spectrosc*, 78 (2011) 319.
16 Kavimani M, Balachandran V, Narayana B, Vanasundari K & Revathi B, *J Mol Struct*, 1149 (2017) 69.
17 Becke A D, *J Chem Phys*, 98 (1993) 5648.
18 Abdel Ghani N T & Mansour A M, *Inorganica Chim Acta*, 373 (2011) 249.
19 Frisch M J, Trucks G W, Schlegal H B, et al., *Gaussian09, Revision A.02*, Gaussian Inc, Wallingford CT, 2009.
20 Young D C, *Computational Chemistry: A Practical Guide for Applying Techniques to Real World Problems (Electronic),* New York, NY: John Wiley & Sons Ltd, 2001.
21 Sundius T, *MOLVIB (V.7.0): Calculation of Harmonic Force Fields Vibrational Modes of Molecules*, QCPE, Program No. 807, 2002.
22 O'boyle N M, Tenderholt A L & Langner K M, *J Comput Chem*, 29 (2007) 839.
23 Lakka N S, Kuppan C, Vadagam N, Ravinathan P, Chepuri K & Chinnakadoori S R, *J Mol Struct*, 1293 (2023) 136159.
24 BIOVIA D S, *Discovery Studio Modeling Environment; Release 2017*, Dessault Systemes, San Diego, CA, USA, 2017.
25 Kim S, Thiessen P A, Bolton E E, Chen J, Fu G, Gindulyte A, Han L, He J, He S, Shoemaker B A, Wang J, Yu B, Zhang J & Bryant S H, *Nucleic Acids Res*, 44 (2015) D1202.
26 Trott O & Olson A J, *J Comput Chem*, 31 (2009) 455.
27 Jia C Y, Li J Y, Hao G F & Yang G F, *Drug Discov Today*, 25 (2020) 248–258.
28 Jian F F, Yu H Q, Qiao Y B, Zhao P S & Xiao H L, *Acta Cryst Section E*, 62 (2006) o3608.
29 Borba A, Albrecht M, Gómez-Zavaglia A, Lapinski L, Nowak M J, Suhm M A & Fausto R, *Phys Chem Chem Phys*, 10 (2008) 7010.
30 Jeyavijayan S, *J Mol Struct*, 1085 (2015) 137.
31 Jeyavijayan S, Ramuthai M & Murugan P, *Asian J Chem*, 34 (2022) 879.
32 Šebek J, Knaanie R, Albee B, Potma E O & Gerber R B, *J Phys Chem A*, 117 (2013) 7442.
33 Sas E B, Kurt M, Karabacak M, Poiyamozhi A & Sundaraganesan N, *J Mol Struct*, 1081 (2015) 506.
34 Jeyavijayan S, *Indian J Pure & Appl Phys,* 54 (2016) 269.
35 Tagore S S, Swaminathan J, Manikandan D, Gomathi S, Nirmal Ram S, Ramalingam M & Sethuraman V, *Chem Phys Letts*, 739 (2020) 136943.
36 Jeyavijayan S & Arivazhagan M, *Indian J Pure & Appl Phys,* 50 (2012) 623.
37 Viji A, Vijayakumar R, Balachandran V, Vanasundari K & Janaki M, *Indian J Chem Tech*, 29 (2022) 616.
38 Sundaraganesan N, Anand B & Dominic Joshua B, *Spectrochim Acta A Mol Biomol Spectrosc*, 65 (2006) 1053.
39 Ramuthai M, Jeyavijayan S, Premkumar R, Uma Priya M & Jayram N D, *J Comput Biophys Chem*, 21 (2022) 219.
40 Costa R A, Junior E S A, Lopes G B P, Pinheiro M L B, Costa E V, Bezerra D P & Oliveira K, *J Mol Struct*, 1171 (2018) 682.
41 Jeyavijayan S, *Spectrochim Acta A Mol Biomol Spectrosc*, 136 (2015) 553.
42 Khalid M, Anwer W, Adeel M, Shafiq Z, Braga A A C, Assiri M A, Imran M & Ullah A, *RSC Adv*, 12 (2022) 29010.
43 Ramuthai M, Jeyavijayan S & Jayram N D, *Polycycl Aromat Compd*, 42 (2021) 6988.
44 Senthilkumar J, Jeyavijayan S & Arivazhagan M, *Spectrochim Acta A Mol Biomol Spectrosc*, 136 (2015) 234.
45 Diwaker, *Spectrochim Acta A Mol Biomol Spectrosc*, 136 (2015) 1932.

46 Abraham C S, Prasana J C, Muthu S, Rizwana B F & Raja M, *J Mol Struct*, 1160 (2018) 393.
47 Rohling R Y, Tranca I C, Hensen E J M & Pidko E A, *J Phys Chem C*, 123 (2019) 2843.
48 Saji R S, Prasana J C, Muthu S & George J, *Heliyon*, 7 (2021) e07213.
49 Ghafoor S, Mansha A, Asim S, Usman M, Zahoor A F & Ali H S, *J Theor Comput Chem*, 19 (2020) 2050020.
50 Pramodh B, Naresh P, Naveen S, Lokanath N K, Ganguly S, Panda J, Murugesan S, Raghu A V & Warad I, *Chem Data Collect*, 31 (2021) 100587.
51 Arivazhagan M, Manivel S, Jeyavijayan S & Meenakshi R, *Spectrochim Acta A Mol Biomol Spectrosc*, 134 (2015) 493.
52 Ayers P W & Parr R G, *J Am Chem Soc*, 122 (2000) 2010.
53 Raja M, Raj Muhamed R, Muthu S & Suresh M, *J Mol Struct*, 1141 (2017) 284.
54 Morell C, Grand A & Toro-Labbé A, *J Phys Chem A*, 109 (2004) 205.
55 Aman H, Rashid N, Ashraf Z, Bibi A, Chen H T & Sathishkumar N, *Heliyon*, 6 (2020) e05187.
56 Mary Y S, Varghese H T, Panicker C Y, Girisha M, Sagar B K, Yathirajan H S, Al-Saadi A A & Van Alsenoy C, *Spectrochim Acta A Mol Biomol Spectrosc*, 150 (2015) 543.
57 Raajaraman B, Sheela N R & Muthu S, *Comput Bio Chem*, 82 (2019) 44.
58 Fizer M, Slivka M, Korol N & Fizer O, *J Mol Struct*, 1223 (2021) 128973.
59 Barfield M & Fagerness P, *J Am Chem Soc*, 119 (1997) 8699.
60 Mosmann T, *J Immunol Methods*, 65 (1983) 55.
61 Abdel Ghani N T & Mansour A M, *Spectrochim Acta A Mol Biomol Spectrosc*, 86 (2012) 605.
62 Abdel Ghani N T & Mansour A M, *Spectrochim Acta A Mol Biomol Spectrosc*, 81 (2011) 529.
63 Christopher Jeyaseelan S, Milton Franklin Benial A & Kaviyarasu K, *J Mol Recognit*. 34(3) (2021) e2873.
64 Meng X Y, Zhang H X, Mezei M & Cui M, *Curr Comput Aided Drug Des*, 7 (2011) 146.
65 Srinivasan S, Sadasivam S K, Gunalan S, Shanmugam G & Kothandan G, *Environ Pollut*, 248 (2019) 599.
66 Mali S N & Pandey A, *J Comput Biophys Chem*, 20 (2021) 267.
67 Govindammal M & Prasath M, *Heliyon*, 6 (2020) e04641.
68 Sakkiah S, Meganathan C, Sohn Y S, Namadevan S & Lee K W, *Int J Mol Sci*, 13 (2012) 5138.